

1 **Unveiling the Dominant Control of the Systematic Cooling Bias in**
2 **CMIP6 Models: Quantification and Corrective Strategies**

3 Jie Zhang^{1,2*}, Kalli Furtado^{3*}, Steven T. Turnock^{4,5}, Yixiong Lu^{1,2}, Tongwen Wu^{1,2},
4 Fang Zhang^{1,2}, Xiaoge Xin^{1,2}, Yuyun Liu⁶

5

6 1. *State Key Laboratory of Disaster Weather Science and Technology, CMA EMPC*
7 2. *CMA Earth System Modeling and Prediction Centre, China Meteorological Administration, Beijing,*
8 *China*
9 3. *National Oceanography Center, Southampton, UK*
10 4. *Met Office Hadley Centre, Exeter, UK*
11 5. *University of Leeds Met Office Strategic (LUMOS) Research Group, University of Leeds, Leeds, UK*
12 6. *Center for Monsoon System Research, Institute of Atmospheric Physics, Chinese Academy of*
13 *Sciences, Beijing, China*

14

15 Corresponding to: Jie ZHANG (jiezhang@cma.gov.cn) & Kalli Furtado (kalli.furtado@noc.ac.uk)

16

17 **Abstract**

18 Including sophisticated aerosol schemes in the models of the sixth Coupled Model
19 Inter-comparison Project (CMIP6) has not improved historical climate simulations. In
20 particular, the models underestimate the surface air temperature anomaly (SATa) when
21 anthropogenic sulfur emissions increased in 1960-1990, making the reliability of the
22 CMIP6 projections questionable. This cooling bias is largely attributable to the
23 unreasonable simulated atmospheric sulfate burden changes. Sulfate burden anomaly
24 are closely linked to both sulfate and SO₂ deposition processes. Intensified sulfate
25 deposition directly reduces atmospheric sulfate loading, while enhanced SO₂ deposition
26 limits precursor availability for sulfate formation by oxidation. These deposition
27 processes regulate sulfate concentrations directly and indirectly. The systematically
28 underestimated sulfate turnover time in CMIP6 models suggests that refining SO₂
29 deposition process rather than sulfate deposition would be a more scientific approach
30 for model improvement. This is supported by two post-CMIP6 models that show better
31 SATa reproduction after improving the SO₂ deposition parameterizations. Strong
32 correlations between sulfate burden anomaly and SATa persist before, during, and after
33 the 1960-1990 period. Such temporal consistency confirms the dominant role of sulfate-
34 related physical processes across all examined time intervals.

36 **1. Introduction**

37 Atmospheric aerosols have rapidly increased since the Industrial Revolution. Over
38 this time period, the total aerosol effective radiative forcing (ERF) was dominated by
39 the sulfate cooling effect, which offsets a substantial portion of global-mean forcing
40 from well-mixed greenhouse gases (IPCC, 2023). Without this historical aerosol ERF,
41 the Paris Agreement's target of limiting global warming to 1.5°C above pre-industrial
42 levels would have already been missed in 2015 (Hienola et al., 2018). Similarly,
43 stopping all present-day anthropogenic aerosol emissions is estimated to induce a
44 global-mean surface heating of 0.5-1.1°C (Samset et al., 2018). The year 2024 has been
45 confirmed as the hottest year in human history and was the first year to breach the 1.5°C
46 warming limit (Bevacqua et al., 2025). Moreover, recent accelerated temperature trends
47 may be attributable to reductions in atmospheric aerosols, particularly from reduced
48 commercial shipping emissions. Hansen et al. (2025) suggest that even small emissions
49 in relatively pristine air have substantial effects, highlighting the crucial need to
50 improve the representation of aerosol effects in global climate models for more reliable
51 projections.

52 The observed temporal evolution of historical surface air temperature (SAT) is one
53 of the major metrics used for evaluating the performance of climate models. However,
54 the SAT anomalies (SATa) in the CMIP6 models are systematically lower than
55 observations during the 1960-1990 period, whereas the CMIP5 models, on average,
56 track the instrumental record quite well (e.g., Flynn and Mauritsen, 2020). The 1960-
57 1990 period, when the cooling bias prevailed, is coincident with the so-called Great
58 Acceleration period, during which human activities intensified remarkably and led to
59 global-scale impacts on the Earth System (Steffen et al., 2007). Recent studies
60 hypothesized that aerosol forcing in CMIP6 is stronger than in CMIP5 and is
61 responsible for the suppressed late 20th-century warming (e.g., Dittus et al., 2020; Smith
62 and Forster, 2021).

63 Given that all CMIP6 models use identical anthropogenic SO₂ emissions (Hoesly et
64 al., 2018), the cooling anomaly points towards a problem with the sulfur cycle in recent

65 earth system models or the emissions data (Hardacre et al., 2021; Wang et al., 2021).
66 In this study, we examine the sulfate-related processes in eleven CMIP6 models with
67 aerosol schemes. We will identify the key processes governing sulfate burden in these
68 models and provide recommendations for further model improvements.

69

70 **2. Model, data, and method**

71 **2.1 CMIP6 models and data**

72 **Table 1.** Information of the eleven CMIP6 models with aerosol schemes.

Model	Country	Interactive Chemistry	Members	Reference
BCC-ESM1	China	Yes	3	Wu et al., (2020); Zhang et al., (2021b)
CESM2	US	No	11	Danabasoglu et al. (2020)
CESM2-FV2	US	No	3	Danabasoglu et al. (2020)
EC-Earth3-AerChem	European consortium	Yes	2	Döscher et al. (2021)
GFDL-ESM4	US	Yes	3	Dunne et al. (2020)
MIROC6	Japan	No	50	Tatebe et al. (2019)
MIROC-ES2L	Japan	No	30	Hajima et al. (2020)
MPI-ESM-1-2-HAM	Germany	Yes	3	Mauritsen et al. (2019)
MRI-ESM2-0	Japan	Yes	10	Yukimoto et al. (2019)
NorESM2-LM	Norway	Yes	3	Seland et al. (2020)
UKESM1-0-LL	UK	Yes	19	Sellar et al. (2019)

73

74 Eleven CMIP6 climate models with interactive aerosol schemes are employed in
75 this study, including seven models with interactive chemistry and four without (Table
76 1). The outputs from two CMIP6 experiments are used: (1) the historical experiment,
77 which simulates climate evolution from 1850 to 2014, forced by time-varying external
78 forcings from natural processes (e.g., solar activity, volcanic eruptions) and
79 anthropogenic factors (e.g., greenhouse gas, aerosol emissions, land-use changes). All
80 the available realizations for each model were used to minimize the uncertainty from
81 internal variability in the climate system; (2) the 1pctCO₂ simulations, in which CO₂ is
82 gradually increased at a rate of 1% per year. The 1pctCO₂ experiment is designed for
83 studying model responses to CO₂ and is somewhat more realistic than rapidly
84 increasing CO₂, such as in the abrupt-4×CO₂ experiment. Historical experiment outputs
85 from two post-CMIP6 models, BCC-ESM1-1 and UKESM1-1-LL, with revised SO₂
86 deposition parameterizations are also included in this study.

87 The model outputs used in this study include SAT and eight key sulfur-cycle
88 variables: sulfate aerosol concentration, sulfate wet and dry deposition rates, sulfur
89 dioxide concentration (SO₂), SO₂ wet and dry deposition rates, gas-phase and aqueous-
90 phase oxidations of SO₂ to sulfate particles. For these sulfur-cycle variables, the inter-
91 member variability within the historical experiment is substantially smaller than that of
92 SAT. For instance, across the 11 CESM2 members, the standard deviation of sulfate
93 burden is only about 4% of its interannual variability during 1960-1990, whereas the
94 corresponding value for SAT is approximately 21%. Similar results are also evident in
95 the 19 UKESM1 members, where the standard deviation of sulfate burden is 3% of its
96 interannual variability, compared to 32% for SAT. Given that inter-member variability
97 in sulfur-cycle variables is relatively small relative to their interannual fluctuations, we
98 therefore use the first realization of the historical simulations and neglect inter-member
99 differences for these sulfur-cycle variables.

100 Monthly mean SAT from the Met Office Hadley Centre/Climatic Research Unit
101 global surface temperature dataset version 5 (HadCRUT5) from 1850 to 2014 are used
102 for model evaluations (Morice et al., 2021). Considering the scarcity of long-term

103 reliable observations in polar regions, we focus on SAT changes within the latitudinal
104 belt from 60°S to 65°N. The ‘global’ mean SAT is calculated as the area-weighted
105 average over this latitudinal belt.

106

107 **2.2 SO₂ turnover time and sulfate turnover time**

108 Atmospheric sulfate concentrations are governed by the emission and oxidation of
109 its precursors, as well as deposition processes. Anthropogenic SO₂ emissions are the
110 major source of sulfate aerosol over land in polluted regions. Given that CMIP6 models
111 typically employ identical anthropogenic SO₂ emission inventories, the inter-model
112 spread in simulated sulfate concentrations primarily stems from discrepancies in SO₂-
113 to-sulfate oxidation rates and sulfate deposition velocities. Here we define the
114 atmospheric residence time of SO₂ and sulfate aerosols as follows.

115 SO₂ turnover time is determined by its atmospheric burden and its total loss rate,
116 which includes both deposition and chemical oxidation to sulfate. It is defined as:

117
$$\tau_{SO_2} = \frac{B_{SO_2}}{(R_{dSO_2} + R_{oSO_2})} \quad (1),$$

118 where τ_{SO_2} is the SO₂ turnover time, B_{SO_2} is the global mean atmospheric SO₂ burden,
119 R_{dSO_2} is the total SO₂ deposition rate including both wet and dry depositions, and R_{oSO_2}
120 is the oxidation rate of SO₂ to sulfate via gas-phase and aqueous-phase chemistry.

121 Sulfate turnover time is defined as:

122
$$\tau_{SO_4} = \frac{B_{SO_4}}{R_{dSO_4}} \quad (2),$$

123 where τ_{SO_4} is the sulfate turnover time, B_{SO_4} is the global mean atmospheric sulfate
124 burden, and R_{dSO_4} is the global mean total sulfate deposition rate including both wet
125 and dry depositions.

126

127 **2.3 The transient Climate Response (TCR) index**

128 The Transient Climate Response (TCR) index is calculated as the mean SAT
129 anomaly over a 20-year period centered on the year when atmospheric CO₂
130 concentration has doubled in the 1pctCO₂ simulation. It is an important metric for
131 quantifying CO₂-induced historical warming and has been widely used for model
132 evaluations and intercomparison studies (e.g., Bevacqua et al., 2025; O'Neill et al.,
133 2016).

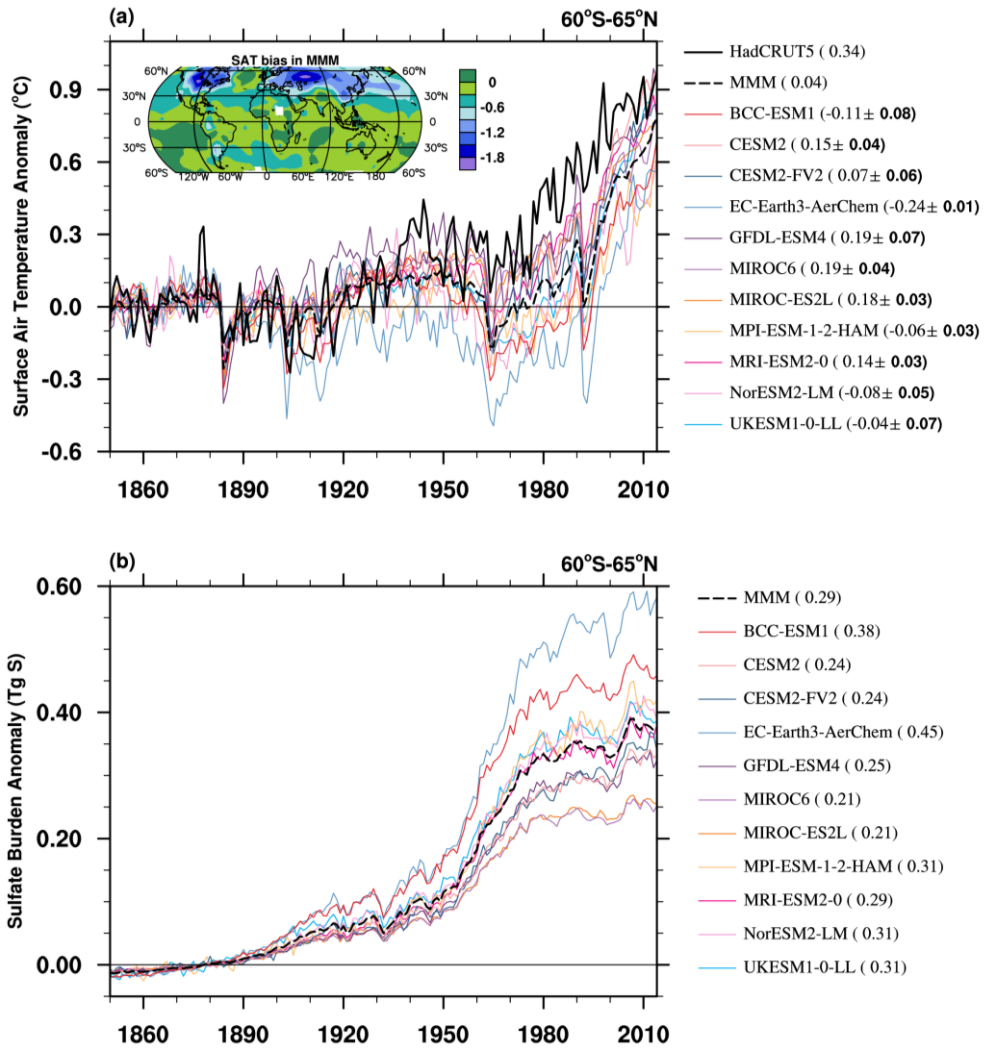
134

135 **3. Results**

136 **3.1 SATa and sulfate burden anomaly**

137 The historical evolutions of global mean SATa in the eleven CMIP6 models with
138 interactive aerosol schemes are shown in Fig. 1a. All the models tend to underestimate
139 SATa since the 1930s. The cooling anomaly in the CMIP6 model marked a notable
140 departure from earlier model generations, which can effectively capture the
141 instrumental SAT record with observations falling well within model spread (e.g.,
142 Flynn and Mauritsen, 2020; Hegerl, et al., 2007).

143 The cooling bias is most pronounced from 1960 to 1990. The SATa is about
144 0.34°C in the observations. However, the multi-model mean (MMM) SATa is about
145 0.3°C lower with a large model spread. The SATa ranges from -0.24°C in EC-Earth3-
146 AerChem to 0.19°C in GFDL-ESM4 and MIROC6. The cooling is noticeable at the
147 mid to high latitude in the Northern Hemisphere (as shown in the attached SATa map
148 in Fig.1a). The sudden drop in SATa in the early 1960s and 1990s may be due to the
149 stronger model responses to large volcanic eruptions, Mount Agung in 1963 and Mount
150 Pinatubo in 1991, than in the observations (Chylek et al., 2020). The cooling biases
151 diminish in later periods, corresponding to the generally high model sensitivity to
152 greenhouse gas forcing (Smith and Forster, 2021).



153

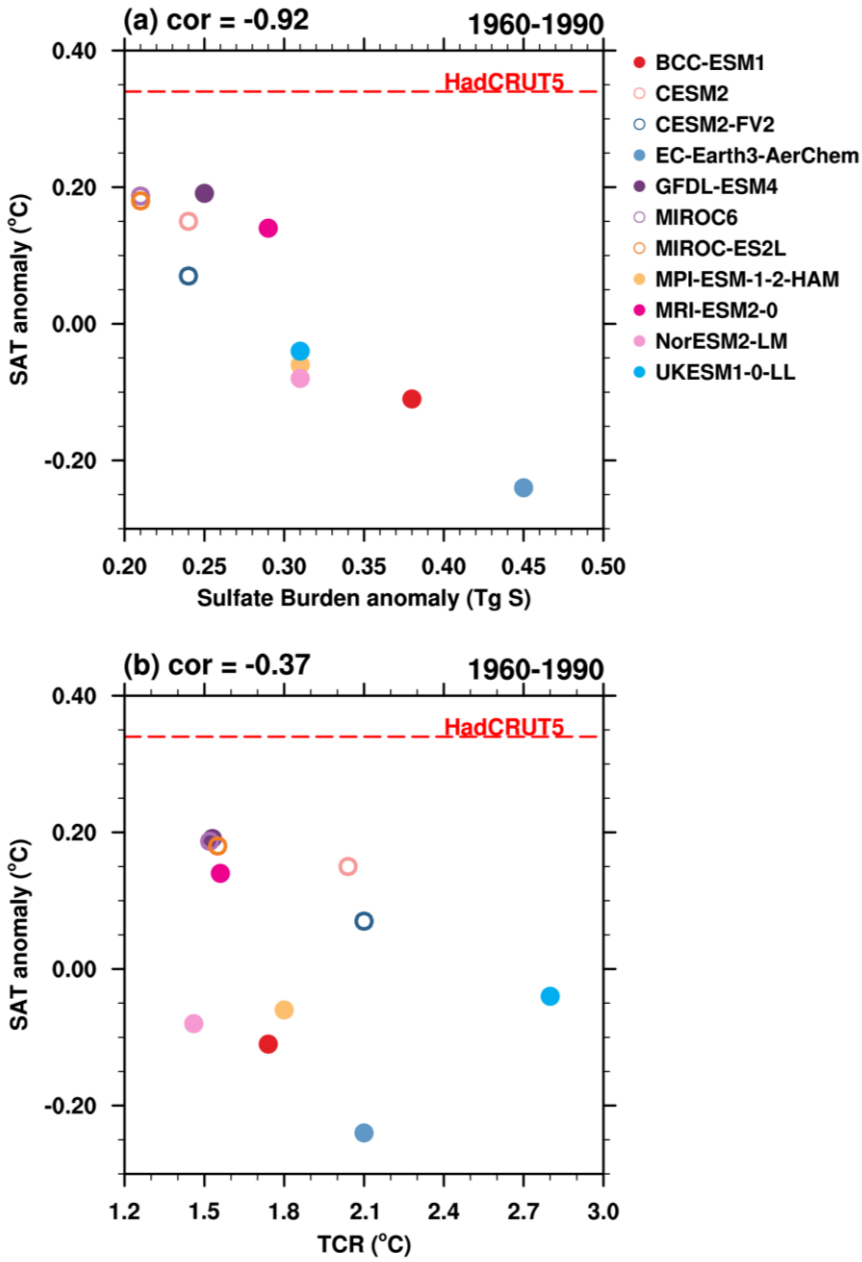
154 **Figure 1.** (a) Historical surface air temperature anomalies (SATa) relative to 1850-1900 mean from
 155 HadCRUT5 (thick black line), the ensemble mean of each CMIP6 model (solid colored lines), and
 156 the multi-model mean (MMM; dashed black line). Numbers in parentheses indicate the mean SATa
 157 for each model during 1960-1990, with the inter-member spread shown as \pm one standard deviation.
 158 Units: $^{\circ}\text{C}$. (b) Same as (a), but for sulfate burden anomalies for the first realization of each CMIP6
 159 model (colored lines) and the MMM (dashed black line). Units: Tg S.

160 The cooling bias in CMIP6 models coincides with the rapid increase in
 161 anthropogenic emissions, particularly of SO_2 , the primary precursor of atmospheric
 162 sulfate (Zhang et al., 2021a). Global SO_2 emissions grew steadily after the 1950s and
 163 peaked in the 1970s at approximately 180Tg yr^{-1} , about 3.6 times the level of the 1950s
 164 (Hoesly et al., 2018). The rise in SO_2 emissions has directly contributed to elevated
 165 sulfate concentrations in the troposphere. The temporal evolution of sulfate burden
 166 shows a significant upward trend aligned with the anthropogenic emission (Fig.1b),

167 initially driven by industrialization and further accelerated after the 1950s mainly due
168 to intensified anthropogenic SO₂ emission from industries and the energy-
169 transformation sectors (e.g., Ohara et al., 2007; Vestreng et al., 2007). The increased
170 sulfate burden interrupted a decades-long warming trend through the cooling effect of
171 sulfate aerosols, even as atmospheric CO₂ concentrations continued to rise (Wilcox et
172 al., 2013).

173 Due to emission-control policies implemented in Europe and North America (Aas
174 et al., 2019; Hand et al., 2012; Vestreng et al., 2007), such as the Gothenburg Protocol
175 (Eb, 1999) and the 1990 Clean Air Act Amendments in the U.S. (Likens et al., 2001),
176 global anthropogenic SO₂ emissions were suppressed after the 1980s and SAT started
177 to rise rapidly in both observation and model simulations. It should be noted that the
178 CMIP6 emission inventory does not fully capture the early 21st century SO₂ emission
179 reductions in East Asia (Wang et al., 2021). However, this period lies outside the 1960-
180 1990 focus of the present study, and its impact on SAT reproduction is beyond the main
181 scope of this paper.

182 The systematically underestimated SATa suggests an excessively strong sulfate-
183 induced cooling effect in CMIP6 models, as indicated by the contrasting performance
184 of individual models. For instance, the MIROC models exhibit the lowest sulfate
185 burden (0.21 Tg S) and smallest cooling bias relative to observation (0.15°C below
186 HadCRUT5) during 1960-1990, while EC-Earth3-AerChem generates a sulfate burden
187 approximately double that value (0.45 Tg S) and nearly four times the cooling bias
188 (0.58°C below HadCRUT5). Analysis across the 11 CMIP6 models reveals a
189 statistically significant negative correlation of -0.92 between sulfate burden anomalies
190 and SATa (Fig. 2a). This relationship highlights the potential role of overestimated
191 sulfate-induced cooling in driving the inter-model spread of SATa biases.



192

193 **Figure 2.** (a) Scatter plots of sulfate burden anomaly versus SATa, and (b) scatter plot of TCR
 194 versus SATa during 1960-1990 from historical experiments. Anomalies are calculated relative to
 195 the 1850-1900 mean. Models with and without interactive chemistry are denoted by colored dots
 196 and colored circles, respectively. The corresponding correlation coefficient (cor) for each panel is
 197 shown in the upper-left corner. The red dashed line refers to SATa in HadCRUT5.

198 Interactive chemistry may affect sulfate formation and sulfate aerosol burdens in
 199 the atmosphere (Mulcahy et al., 2020). Models with interactive chemistry (colored dots
 200 in Fig.2a) generally show higher sulfate burdens and lower SATa than non-interactive
 201 models (colored circles). However, the relationship between sulfate burden anomaly

202 and SATa is a robust feature across CMIP6 models, independent of their chemical
203 complexity.

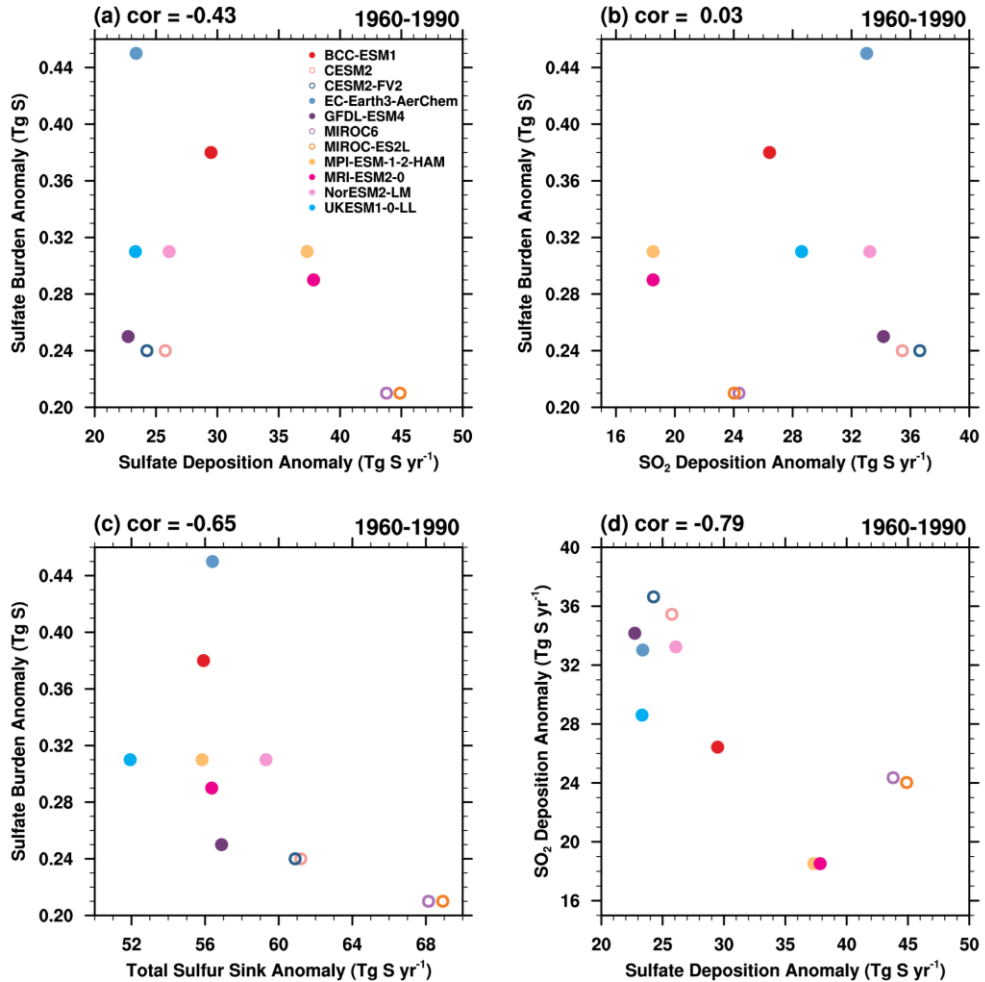
204 Greenhouse gases (GHGs) also increased rapidly during 1960-1990. However,
205 TCR, which can generally indicate the impact of GHGs, is insignificantly correlated
206 with SATa in CMIP6 models, and the correlation coefficient across models is even
207 negative (Fig.2b). Therefore, the inter-model spread in cooling biases can substantially
208 be attributed to discrepancies in simulated sulfate aerosol burden.

209 It should be noticed that there are fast and slow components of global warming in
210 response to radiative forcing changes (Held et al., 2010). The fast component,
211 characterized by an exponential decay timescale of less than 5 years, is primarily driven
212 by rapid adjustments in the upper ocean layers. In contrast, the slow component evolves
213 over centuries and is associated with heat uptake by deeper ocean layers. Lagged
214 oceanic and dynamical feedbacks will further delay and modulate warming rates (Chen
215 et al., 2016; Watterson and Dix, 2005). In this study, the fast response to sulfate forcing
216 can be rapidly detected by SATa, especially when the sulfate forcing is sustained during
217 1960-1990. Moreover, the global mean perspective in this study makes the results
218 insensitive to the impact of spatial redistribution of temperature anomalies caused by
219 dynamical feedbacks.

220

221 **3.2 Sulfur Deposition rates and SO₂ oxidation rate**

222 SO₂ deposition, sulfate deposition, and SO₂ oxidation to sulfate are the key
223 processes governing the atmospheric sulfur cycle. About half of the SO₂ emission is
224 removed by dry deposition at the surface and through wet scavenging by precipitation
225 (e.g., Chin et al., 1996). The remaining fraction is oxidized to sulfate, mainly through
226 two pathways: gas-phase reaction with the hydroxyl radical (OH), and aqueous-phase
227 oxidation within cloud and fog droplets, where reactions with ozone (O₃) and hydrogen
228 peroxide (H₂O₂) are dominant. These processes are critical determinants of atmospheric
229 sulfate burden.

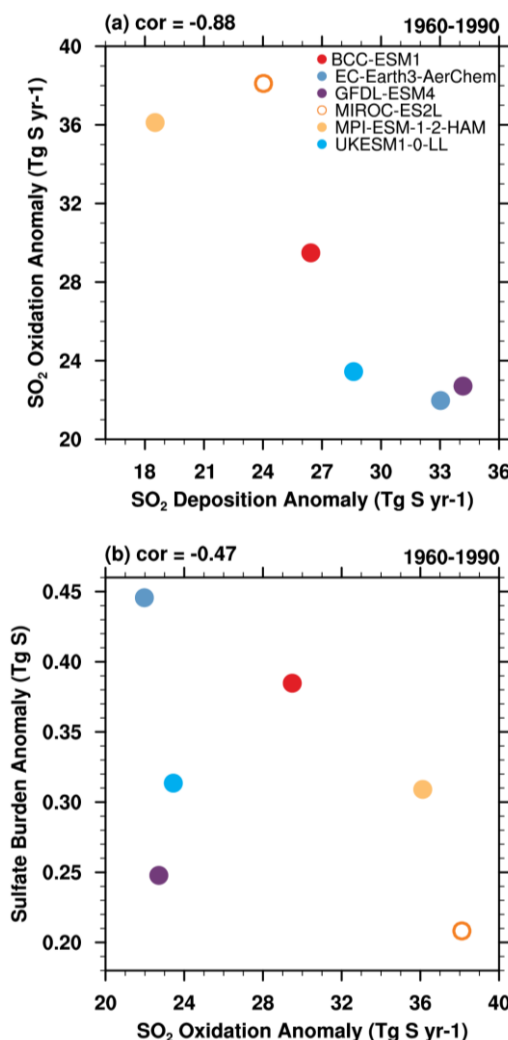


230

231 **Figure 3.** (a) Sulfate deposition anomaly, (b) SO₂ deposition anomaly, and (c) total sulfur sink
 232 anomalies (x-axis) versus sulfate burden anomaly (Tg S, y-axis) in each model during 1960-1990. (d)
 233 Sulfate deposition anomaly (x-axis) versus SO₂ deposition anomaly (y-axis) during 1960-1990.
 234 Units for deposition anomalies are Tg S yr⁻¹.

235 Fig. 3 shows the inter-model relationship between global mean anomalies of
 236 sulfate burdens and sulfur depositions during 1960-1990, relative to the pre-industrial
 237 baseline (1850-1900). The sulfate burden anomaly is negatively correlated with sulfate
 238 deposition anomaly. However, the correlation is statistically insignificant. This may be
 239 partly attributable to a subset of five models characterized by both low sulfate burden
 240 and low sulfate deposition anomalies. These models degrade the robustness of the linear
 241 fit derived from the remaining models. There is no clear statistical relationship between
 242 sulfate burden anomaly and SO₂ deposition anomaly (Fig. 3b). However, when
 243 considering the total sulfur sink anomaly, including both sulfate and SO₂ deposition

244 anomalies, the correlation with sulfate burden anomaly strengthens to -0.65, significant
 245 at the 5% level using a Student's t-test (Fig.3c). Notably, within the subset of five
 246 models, most show higher SO_2 deposition anomaly in relative to the multi-model mean.
 247 This high SO_2 deposition anomaly compensates for their low sulfate deposition
 248 anomaly, influencing the total sulfur deposition magnitude sufficiently to sustain a
 249 significant correlation with sulfate burden anomaly in these models. Further analysis
 250 reveals a strong negative correlation (-0.79) between SO_2 deposition rate anomaly and
 251 sulfate deposition rate anomaly, suggesting a compensatory relationship between these
 252 two sulfur removal pathways (Fig.3d).



253

254 **Figure 4.** (a) SO_2 deposition anomaly versus SO_2 oxidation anomaly, and (b) SO_2 oxidation
 255 anomaly versus sulfate burden anomaly in each model during 1960-1990.

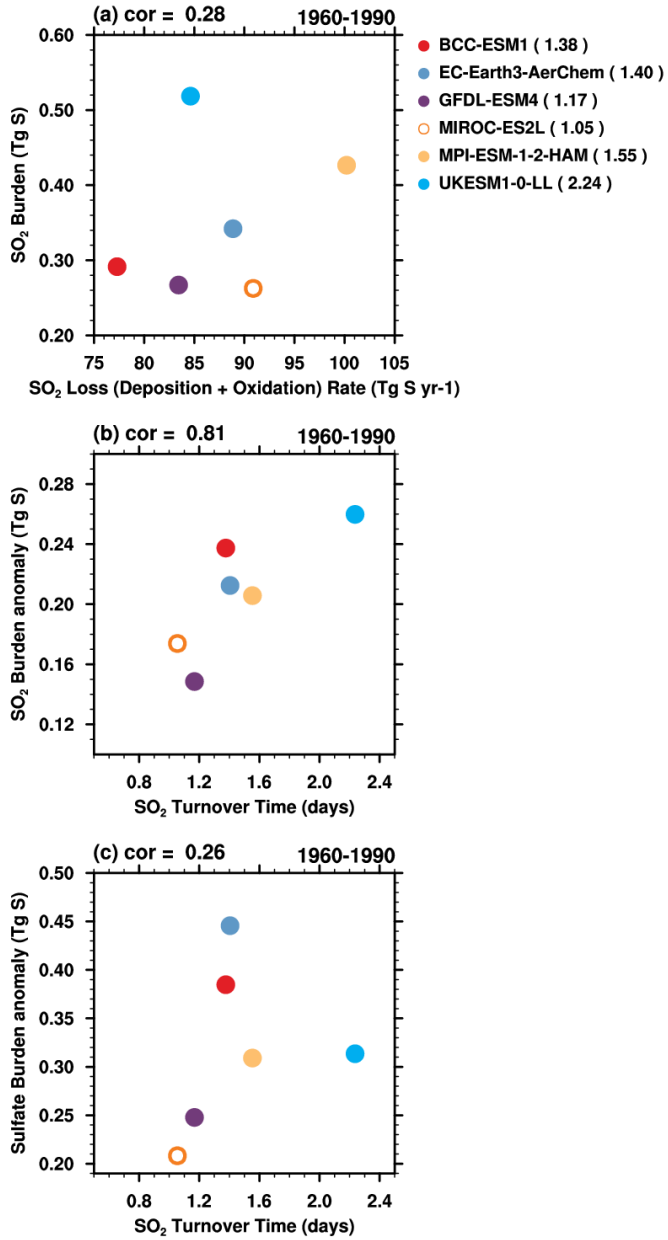
256 The formation of atmospheric sulfate aerosol is governed by the balance between
257 the loss of its precursor, SO_2 , and its chemical transformation. As shown in Fig.4a,
258 inter-model comparisons show a significant anti-correlation between SO_2 deposition
259 anomaly and the oxidation rate anomaly across the six models for which relevant data
260 are available for calculation (-0.88). That is, enhanced SO_2 deposition rate, particularly
261 through dry deposition processes, limits the availability of SO_2 for oxidation to sulfate.
262 The relationship between oxidation rate anomalies and the sulfate burden anomalies is
263 negative but not statistically robust within this limited model subset. A more
264 comprehensive analysis with a larger model ensemble is needed to robustly quantify
265 the relative contributions of oxidation pathways to the sulfate aerosol burden.

266 Therefore, biases in sulfate burden simulations arise either directly from sulfate
267 deposition or indirectly from SO_2 deposition, which limits the availability of SO_2 for
268 oxidation.

269

270 **3.3 SO_2 turnover time and sulfate turnover time**

271 SO_2 deposition, sulfate deposition, and SO_2 oxidation rate determine the respective
272 turnover times for SO_2 and sulfate, which quantify their mean atmospheric residence
273 times before removal. Here we examine SO_2 turnover time and sulfate turnover time,
274 quantities with clear physical interpretations, to identify the dominant physical and
275 chemical processes responsible for the sulfate burden biases.

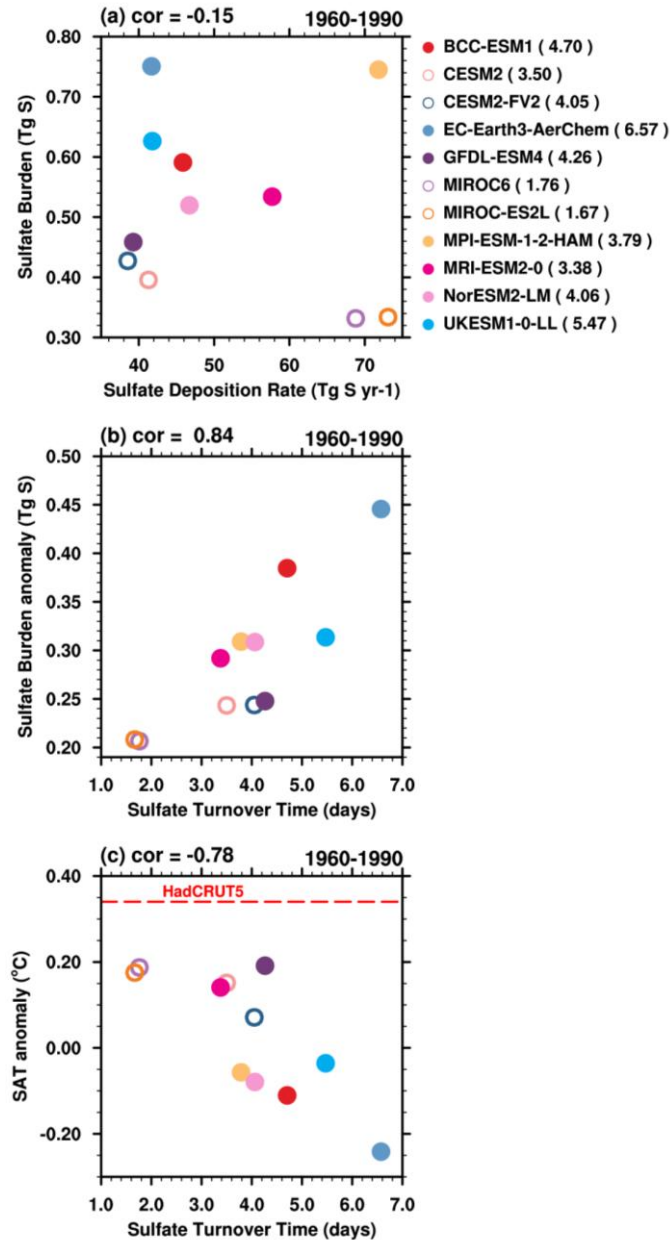


276

277 **Figure 5.** (a) SO_2 loss rate versus SO_2 burden in 1960-1990. SO_2 loss rate includes SO_2 deposition
 278 and oxidation. (b) SO_2 turnover time versus SO_2 burden anomaly in 1960-1990. (c) SO_2 turnover
 279 time versus sulfate burden anomaly in 1960-1990.

280 The correlations between SO_2 burden and its total loss rate, including both
 281 deposition and chemical oxidation, are notably weak (Fig.5a). Given that the models
 282 share identical anthropogenic SO_2 emission inventories, this poor correlation likely
 283 stems from substantial inter-model differences in the representation of natural SO_2
 284 precursor emissions (e.g., from oceanic dimethyl sulfide) and their subsequent

285 atmospheric processing. The SO_2 turnover time (τ_{SO_2}) as defined in Eq. 1, ranges from
 286 1.05 to 2.24 days in the CMIP6 models. The τ_{SO_2} is highly correlated with SO_2 burden
 287 anomaly with a correlation coefficient of 0.81 (Fig.5b). However, its correlation with
 288 the sulfate burden anomaly is weak (Fig.5c).



289

290 **Figure 6.** (a) Sulfate deposition rate versus sulfate burden during 1960-1990. (b) Sulfate turnover
 291 time versus sulfate burden anomaly during 1960-1990. (c) Sulfate turnover time versus SATa during
 292 1960-1990. The red dashed line refers to SATa in HadCRUT5.

293 Figure 6 presents the simulated sulfate deposition and sulfate burden in 1960-1990.
294 The weak negative correlation (-0.15) indicates that sulfate deposition alone cannot
295 fully explain inter-model differences in sulfate burden. Sulfate turnover time is
296 quantified following Eq. (2) in Section 2.2 as the ratio of sulfate burden to sulfate
297 deposition, representing the average atmospheric residence time of sulfate aerosols.
298 The sulfate turnover time exhibits considerable inter-model variability, ranging from
299 1.67 days in MIROC-ES2L to 6.57 days in EC-Earth3-AerChem. These results
300 generally agree with most aerosol models, which typically simulate sulfate lifetimes
301 of around 4 days (e.g., Textor et al., 2006; Liu et al., 2012; Matsui and Mahowald,
302 2017; Tegen et al., 2019). However, sulfate turnover times in models are notably
303 shorter than observational estimates, such as 7.3 days (0.02 yr) in Charlson et al.
304 (1992) and 10-14 days in Kristiansen et al. (2012). This discrepancy may stem from
305 premature removal processes, inadequate poleward transport, or incomplete chemical
306 representations (e.g., Croft et al., 2014).

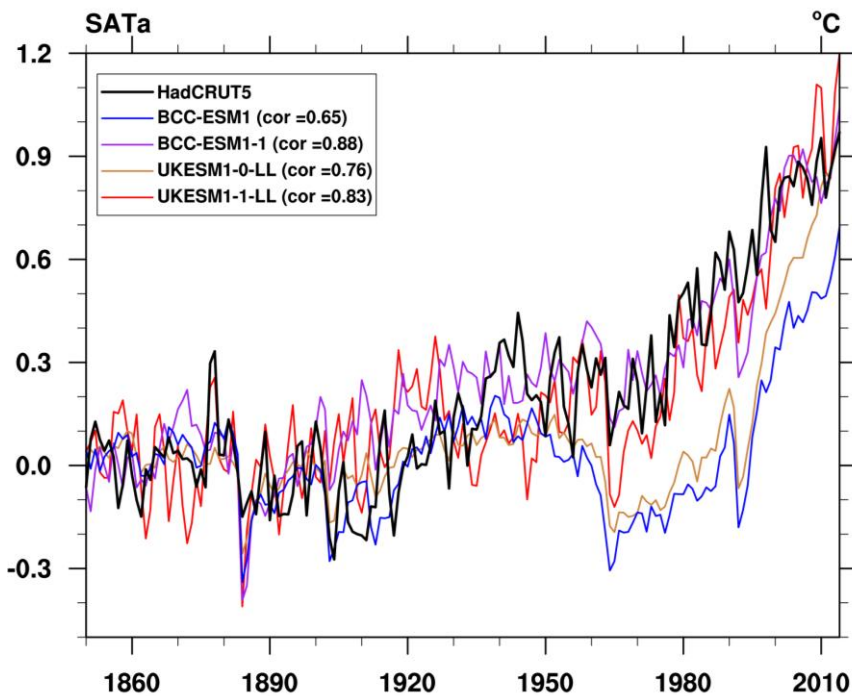
307 The inter-model variations in sulfate turnover time exhibit a strong correlation with
308 sulfate burden anomalies and SATa during the 1960-1990 period, with a correlation
309 coefficient of 0.84 and -0.78 (Fig.6b and Fig.6c). This suggests that differences in
310 sulfate turnover time may account for both the sulfate burden anomaly variations and
311 the consequent surface temperature differences among models. CMIP6 models
312 systematically overestimate sulfate burden anomalies, implying that these models
313 should exhibit shorter lifetimes to produce lower sulfate burden anomalies and higher
314 SATa (Fig.6c). However, enhancing sulfate deposition to reduce burden anomalies is
315 not a physically reasonable solution, as it would worsen the already too-short
316 simulated sulfate aerosol lifetime.

317 Therefore, as indicated by section 3.2, model improvement efforts should
318 prioritize SO₂ deposition process refinement rather than sulfate deposition adjustment
319 as a more scientifically sound approach.

320

321 **3.4 The performances in the two post-CMIP6 models**

322 To suppress the substantial cold bias in the BCC-ESM1 model, which
323 underestimates the observed SATa by 0.45°C during the 1960-1990 period, we increase
324 the dry deposition velocity of SO₂ by a factor of four over land surface and by a factor
325 of 1.5 over the ocean to reduce the availability of SO₂ for oxidation. This effect is
326 similar to that in UKESM1-0-LL by improving SO₂ dry deposition parameterization
327 (Hardacre et al., 2021; Mulcahy et al., 2023). The impact of changes to the SO₂ dry
328 deposition parameterization in UKESM1-0-LL is an increase of SO₂ dry deposition by
329 a factor of 2 to 4. Accordingly, SATa increases to 0.45°C in BCC-ESM1-1 and rises to
330 0.25°C in UKESM1-LL. Sulfate turnover time in the two post-CMIP6 models, 8.53
331 days in BCC-ESM1-1 and 5.77 days in UKESM1-1-LL, is generally longer than that
332 of their CMIP6 versions. The longer sulfate lifetimes in the two post-CMIP6 models
333 may be due to lower SO₂ in these revised models, but also could be due to physical
334 climate changes (e.g., temperatures, clouds, rainfall).

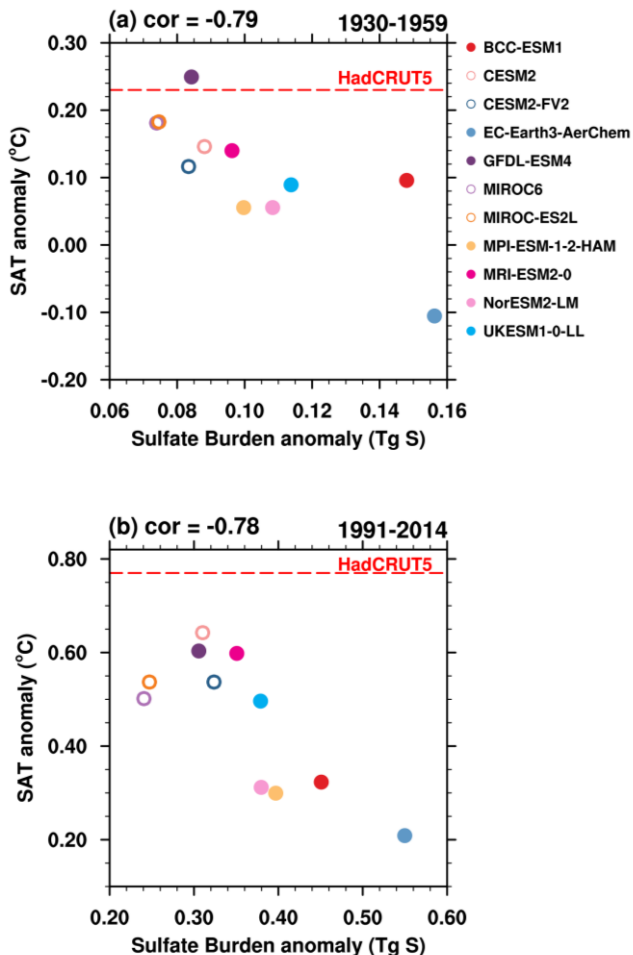


336 **Figure 7.** Evolutions of SATa relative to 1850-1900 mean for HadCRUT5, BCC-ESM models, and
337 UKESM models. The numbers in legend are the corresponding correlation coefficients with
338 HadCRUT5.

339 As demonstrated by the global mean SATa in BCC-ESM1-1 and UKESM1-1-LL
 340 (Fig.7), both models on average tracked the instrumental record quite well with
 341 statistically higher correlation coefficients with observation (HadCRUT5). That is,
 342 improvements in SO_2 deposition parameterizations have contributed to better model
 343 performances in reproducing historical surface temperature evolution.

344

345 **3.5 Relative changes preceding and following the 1960-1990 period**

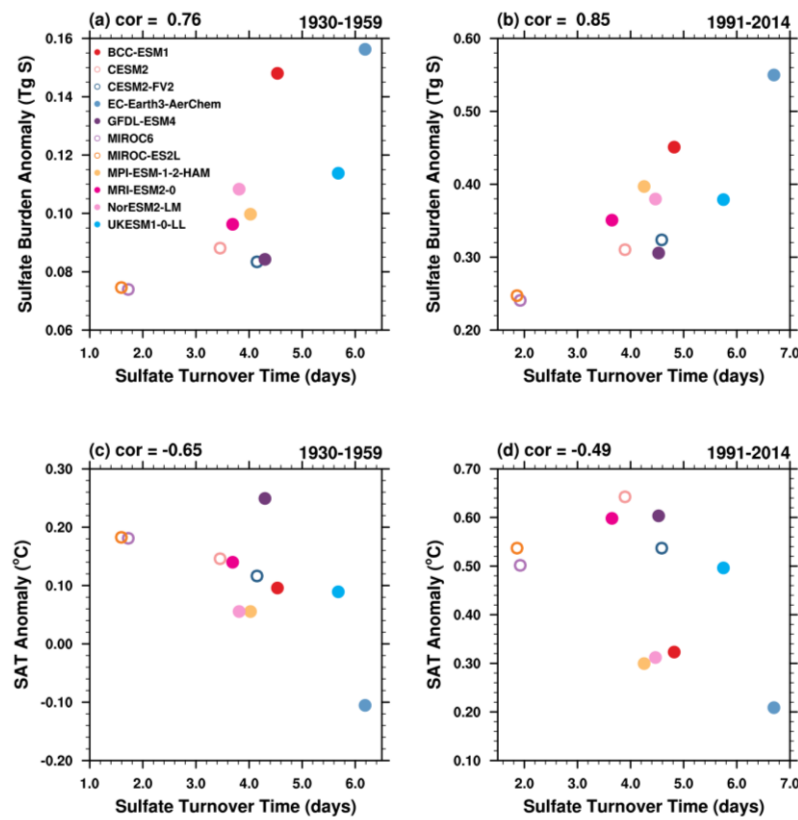


346

347 **Figure 8.** Scatter plots of sulfate burden anomalies versus SATa in (a) 1930-1959, and (b) 1991-
 348 2014.

349 Our analysis reveals a robust correlation between sulfate burden anomalies and
 350 SATa during 1960-1990 (Fig. 2a). To evaluate the temporal consistency of this

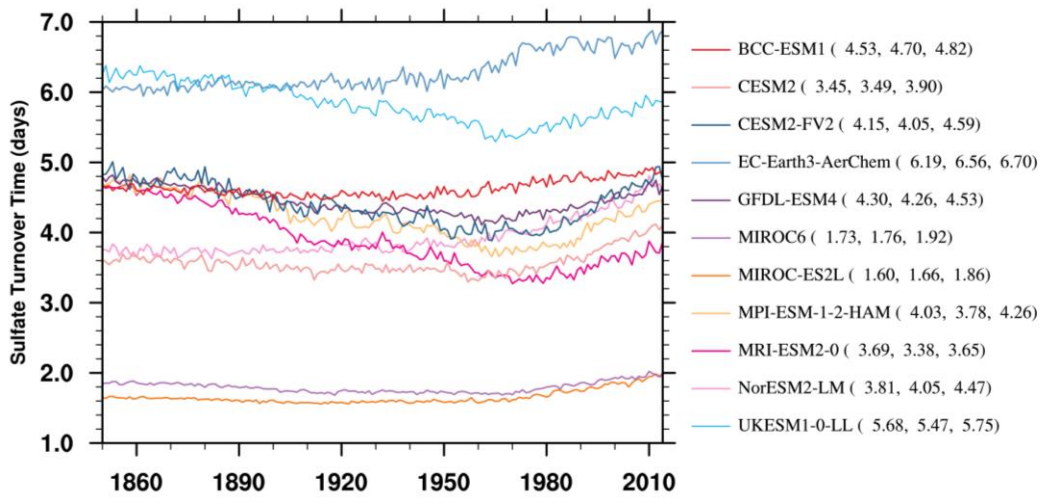
relationship, we examined its behavior before and after this period. Given that the relationship reflects clear underlying physics, similar correlations were expected across different periods. As shown in Fig.8, statistically significant correlations are evident in both periods, suggesting that sulfate burden anomalies were overestimated prior to 1960-1990, and this overestimation continued to influence SATa in subsequent decades. Compared to HadCRUT5, the models on average underestimate SATa by 0.11°C during 1930-1959 and by 0.31°C during 1991-2014. The correlations between sulfate burden anomalies and SATa are -0.79 and -0.78 for these two periods, respectively, which are weaker than the correlation of -0.91 during 1960-1990. This weakening may be partly attributable to the smaller biases in the 1930-1959 interval. Furthermore, the combined effects of increasing atmospheric CO₂ concentrations since the Industrial Revolution and the high climate sensitivity in CMIP6 models may have partially offset the cooling bias during 1991-2014 (Hausfather et al., 2022).



364

365 **Figure 9.** Sulfate turnover time (τ_{SO_4}) versus (a, b) sulfate burden anomalies, and (c, d) SATa for
366 the periods 1930-1959 and 1991-2014.

367 Sulfate turnover time is a key parameter governing sulfate burden and shows
 368 strong correlations with sulfate burden anomalies and SATa during 1960-1990 (Figs.
 369 6b and 6c). Statistically significant correlations persist before and after this period (Fig.
 370 9), confirming the dominant role of sulfate-related physical processes across all
 371 examined time intervals.

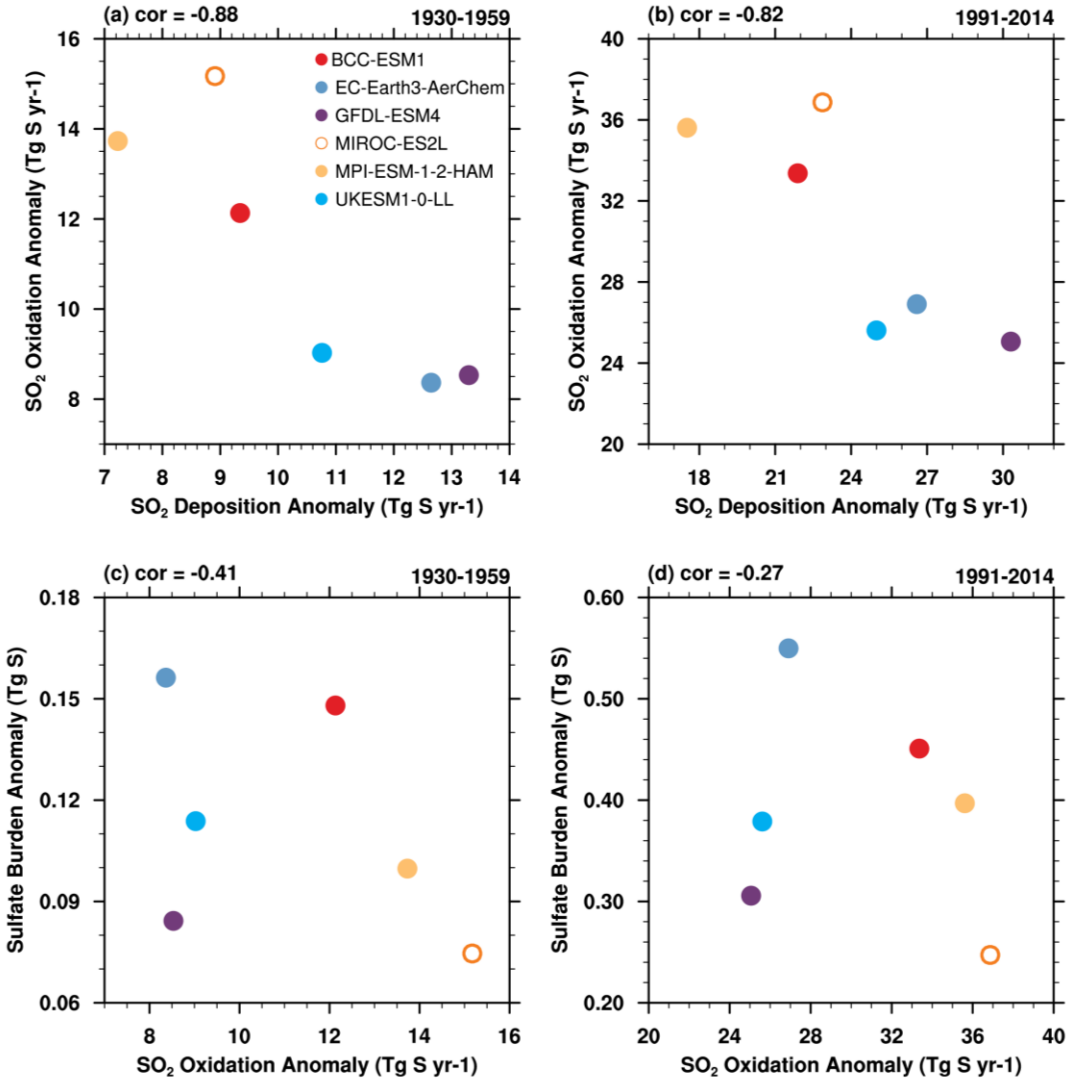


372

373 **Figure 10.** Temporal evolution of sulfate turnover time (τ_{SO_4}) in CMIP6 models. Numerical labels
 374 denote mean τ_{SO_4} value during 1930-1959, 1960-1990, and 1991-2014.

375

376 We also analyze the temporal evolution of sulfate turnover time (Fig.10). Its
 377 temporal variability, characterized by a standard deviation ($\sigma < 0.5$ days), is notably
 378 smaller than the inter-model spread. During 1930-1959, models exhibit a divergent
 379 trend, with 5 out of 11 models simulating reduced turnover times in the subsequent
 380 period. In contrast, all models show prolonged turnover times during 1991-2014
 381 compared to earlier periods. This shift may be partly attributable to changes in the
 382 regional distribution of sulfur emissions, including an increasing proportion of
 383 emissions from Asia and the implementation of stringent emission control policies in
 384 Europe and North America.



385

386 **Figure 11.** Same as Fig.4, but for (a, c) 1930-1959, and (b, d) 1991-2014.

387 SO_2 deposition maintains a strong negative correlation with SO_2 oxidation both
 388 before and after the 1960-1990 period (Fig.11), with coefficients of -0.88 and -0.82,
 389 respectively. Meanwhile, the anomaly in SO_2 oxidation exhibits a negative but
 390 statistically insignificant correlation with the sulfate burden anomaly.

391

392 **4. Conclusions**

393 The aerosol cooling effect is considered as the second most important
 394 anthropogenic forcing during the 20th Century. Based on the 11 CMIP6 models with
 395 interactive aerosol schemes, our study demonstrates that the cooling bias during 1960-

396 1990 is closely related to the sulfate burden changes in the atmosphere. Sulfate aerosol
397 represents the terminal product of a complex chain of physicochemical processes that
398 convert sulfur emissions into sulfate particles. Our findings indicate that sulfate burden
399 anomalies in these models are governed by two key processes: the removal of its
400 gaseous precursor SO_2 and sulfate deposition itself. Higher SO_2 deposition rates limit
401 the availability of SO_2 for subsequent oxidations. Sulfate turnover time is critical for
402 evaluating the physical realism of models. Comparative analysis with observational
403 measurements reveals that increasing sulfate deposition to reduce sulfate burden
404 anomalies is not a reasonable approach. Biases in sulfate burden anomalies may be
405 driven by discrepancies in simulating upstream SO_2 deposition and oxidation processes,
406 rather than downstream processes. This is further supported by improvements in two
407 post-CMIP6 models with refined SO_2 deposition parameterizations.

408 Analyses for periods preceding and following 1960-1990 confirm the persistent
409 influence of sulfate-related physical processes across all examined time periods.
410 Therefore, CMIP6 model projections should be interpreted with caution, as they may
411 underestimate future warming rates. It is therefore also essential to evaluate the
412 reliability of sulfate-related processes in upcoming model intercomparisons before
413 applying them to future climate projections. We encourage future intercomparison
414 initiatives to archive sulfur cycle relevant outputs from a wider range of participating
415 models, thereby enabling more robust and comprehensive process-oriented evaluations.

416

417 **Code availability**

418 All data processing codes are available if a request is sent to the corresponding authors.

419

420 **Data availability**

421 The HadCRUT5 dataset is accessible through the Met Office Hadley Centre
422 observations database (<https://www.metoffice.gov.uk/hadobs/hadcrut5/>). All the model
423 data can be freely downloaded from the Earth System Grid Federation (ESGF) nodes
424 (<https://aims2.llnl.gov/search/cmip6/>).

425

426 **Author contributions**

427 The main ideas were formulated by J.Z. and K.F. J.Z. wrote the original draft. The
428 results were supervised by K.F. and S.T.T. All the authors discussed the results and
429 contributed to the final manuscript.

430

431 **Competing interests**

432 The authors declare no competing financial and/or non-financial interests.

433

434 **Acknowledgements**

435 We would like to thank the editors for handling the manuscript and providing
436 constructive guidance throughout the review process. We sincerely appreciate the
437 insightful comments from Dr. Stephen E. Schwartz and the anonymous reviewers,
438 which significantly improved the quality of this work. We acknowledge all data
439 developers, their managers, and funding agencies for the datasets used in this study,
440 whose contributions and support were essential to our research.

441

442 **Financial support**

443 This work was jointly supported by the National Natural Science Foundation of China
444 (Grant no. U2542212 and 42230608) and the UK–China Research and Innovation
445 Partnership Fund through the Met Office Climate Science for Service Partnership
446 (CSSP) China as part of the Newton Fund.

447

448 **References**

449 Aas, W., Mortier, A., Bowersox, V., Cherian, R., Faluvegi, G., Fagerli, H., Hand, J.,
450 Klimont, Z., Galy-Lacaux, C., Lehmann, C. M. B., Myhre, C. L., Myhre, G., Olivié,
451 D., Sato, K., Quaas, J., Rao, P. S. P., Schulz, M., Shindell, D., Skeie, R. B., Stein,
452 A., Takemura, T., Tsyro, S., Vet, R., and Xu, X.: Global and regional trends of
453 atmospheric sulfur, *Scientific Reports*, 9, 953, 10.1038/s41598-018-37304-0,
454 2019.

455 Bevacqua, E., Schleussner, C., and Zscheischler, J.: A year above 1.5 °C signals that
456 Earth is most probably within the 20-year period that will reach the Paris
457 Agreement limit, *Nature Climate Change*, 1-4, 10.1038/s41558-025-02246-9,
458 2025.

459 Charlson, R. J., Schwartz, S. E., Hales, J. M., Cess, R. D., Coakley, J. A., Hansen, J. E.
460 and Hofmann, D. J.: Climate Forcing by Anthropogenic Aerosols, *Science*, 255,
461 423-430. 1992.

462 Chen, J. P., Chen, I. J. and Tsai, I. C.: Dynamic Feedback of Aerosol Effects on the
463 East Asian Summer Monsoon, *Journal of Climate*, 29, 6137-6149. 2016.

464 Chin, M., Jacob, D. J., Gardner, G. M., Foreman-Fowler, M. S., Spiro, P. A. and Savoie,
465 D. L.: A global three-dimensional model of tropospheric sulfate, *Journal of
466 Geophysical Research: Atmospheres*, 101, 18667-18690. 1996.

467 Chylek, P., Folland, C., Klett, J. D., and Dubey, M. K.: CMIP5 Climate Models
468 Overestimate Cooling by Volcanic Aerosols, *Geophysical Research Letters*, 47,
469 e2020GL087047, <https://doi.org/10.1029/2020GL087047>, 2020.

470 Croft, B., Pierce, J. R. and Martin, R. V.: Interpreting aerosol lifetimes using the GEOS-
471 Chem model and constraints from radionuclide measurements, *Atmospheric
472 Chemistry and Physics*, 14, 4313-4325. 2014.

473 Danabasoglu, G., Lamarque, J. F., Bacmeister, J., Bailey, D. A., DuVivier, A. K.,
474 Edwards, J., Emmons, L. K., Fasullo, J., Garcia, R., Gettelman, A., Hannay, C.,
475 Holland, M. M., Large, W. G., Lauritzen, P. H., Lawrence, D. M., Lenaerts, J. T.
476 M., Lindsay, K., Lipscomb, W. H., Mills, M. J., Neale, R., Oleson, K. W., Otto-
477 Bliesner, B., Phillips, A. S., Sacks, W., Tilmes, S., van Kampenhout, L.,

478 Vertenstein, M., Bertini, A., Dennis, J., Deser, C., Fischer, C., Fox-Kemper, B.,
479 Kay, J. E., Kinnison, D., Kushner, P. J., Larson, V. E., Long, M. C., Mickelson,
480 S., Moore, J. K., Nienhouse, E., Polvani, L., Rasch, P. J., and Strand, W. G.: The
481 Community Earth System Model Version 2 (CESM2), *J. Adv. Model. Earth Syst.*,
482 12, 35, 10.1029/2019ms001916, 2020.

483 Dittus, A. J., Hawkins, E., Wilcox, L. J., Sutton, R. T., Smith, C. J., Andrews, M. B.,
484 and Forster, P. M.: Sensitivity of Historical Climate Simulations to Uncertain
485 Aerosol Forcing, *Geophysical Research Letters*, 47, e2019GL085806,
486 10.1029/2019gl085806, 2020.

487 Döscher, R., Acosta, M., Alessandri, A., Anthoni, P., Arneth, A., Arsouze, T.,
488 Bergmann, T., Bernadello, R., Boussetta, S., Caron, L. P., Carver, G., Castrillo, M.,
489 Catalano, F., Cvijanovic, I., Davini, P., Dekker, E., Doblas-Reyes, F. J., Docquier,
490 D., Echevarria, P., Fladrich, U., Fuentes-Franco, R., Gröger, M., v. Hardenberg,
491 J., Hieronymus, J., Karami, M. P., Keskinen, J. P., Koenigk, T., Makkonen, R.,
492 Massonnet, F., Ménégoz, M., Miller, P. A., Moreno-Chamarro, E., Nieradzik, L.,
493 van Noije, T., Nolan, P., O'Donnell, D., Ollinaho, P., van den Oord, G., Ortega,
494 P., Prims, O. T., Ramos, A., Reerink, T., Rousset, C., Ruprich-Robert, Y., Le Sager,
495 P., Schmith, T., Schrödner, R., Serva, F., Sicardi, V., Sloth Madsen, M., Smith, B.,
496 Tian, T., Tourigny, E., Uotila, P., Vancoppenolle, M., Wang, S., Wårldin, D.,
497 Willén, U., Wyser, K., Yang, S., Yepes-Arbós, X., and Zhang, Q.: The EC-Earth3
498 Earth System Model for the Climate Model Intercomparison Project 6, *Geosci.*
499 *Model Dev. Discuss.*, 2021, 1-90, 10.5194/gmd-2020-446, 2021.

500 Dunne, J. P., Horowitz, L. W., Adcroft, A. J., Ginoux, P., Held, I. M., John, J. G.,
501 Krasting, J. P., Malyshev, S., Naik, V., Paulot, F., Shevliakova, E., Stock, C. A.,
502 Zadeh, N., Balaji, V., Blanton, C., Dunne, K. A., Dupuis, C., Durachta, J., Dussin,
503 R., Gauthier, P. P. G., Griffies, S. M., Guo, H., Hallberg, R. W., Harrison, M., He,
504 J., Hurlin, W., McHugh, C., Menzel, R., Milly, P. C. D., Nikonorov, S., Paynter, D.,
505 J., Poshay, J., Radhakrishnan, A., Rand, K., Reichl, B. G., Robinson, T.,
506 Schwarzkopf, D. M., Sentman, L. T., Underwood, S., Vahlenkamp, H., Winton,
507 M., Wittenberg, A. T., Wyman, B., Zeng, Y., and Zhao, M.: The GFDL Earth

508 System Model Version 4.1 (GFDL-ESM 4.1): Overall Coupled Model Description
509 and Simulation Characteristics, *J. Adv. Model. Earth Syst.*, 12,
510 10.1029/2019ms002015, 2020.

511 EB, U.: Protocol to Abate Acidification, Eutrophication and Ground-level Ozone, 1999.

512 Flynn, C. M. and Mauritsen, T.: On the climate sensitivity and historical warming
513 evolution in recent coupled model ensembles, *Atmos. Chem. Phys.*, 20, 7829-7842,
514 10.5194/acp-20-7829-2020, 2020.

515 Hajima, T., Watanabe, M., Yamamoto, A., Tatebe, H., Noguchi, M. A., Abe, M.,
516 Ohgaito, R., Ito, A., Yamazaki, D., Okajima, H., Ito, A., Takata, K., Ogochi, K.,
517 Watanabe, S., and Kawamiya, M.: Development of the MIROC-ES2L Earth
518 system model and the evaluation of biogeochemical processes and feedbacks,
519 *Geoscientific Model Development*, 13, 2197-2244, 10.5194/gmd-13-2197-2020,
520 2020.

521 Hand, J. L., Schichtel, B. A., Malm, W. C., and Pitchford, M. L.: Particulate sulfate ion
522 concentration and SO₂ emission trends in the United States from the early 1990s
523 through 2010, *Atmos. Chem. Phys.*, 12, 10353-10365, 10.5194/acp-12-10353-
524 2012, 2012.

525 Hansen, J., Kharecha, P., Sato, M., Tselioudis, G., Kelly, J., Bauer, S., Ruedy, R., Jeong,
526 E., Jin, Q., Rignot, E., Velicogna, I., Schoeberl, M., Schuckmann, K., Amponsem,
527 J., Cao, J., Keskinen, A., Li, J., and Pokela, A.: Global Warming Has Accelerated:
528 Are the United Nations and the Public Well-Informed?, *Environment: Science and
529 Policy for Sustainable Development*, 67, 6-44, 10.1080/00139157.2025.2434494,
530 2025.

531 Hardacre, C., Mulcahy, J. P., Pope, R. J., Jones, C. G., Rumbold, S. T., Li, C., Johnson,
532 C., and Turnock, S. T.: Evaluation of SO₂, SO₄²⁻ and an updated SO₂ dry
533 deposition parameterization in the United Kingdom Earth System Model,
534 *Atmospheric Chemistry and Physics*, 21, 18465-18497, 10.5194/acp-21-18465-
535 2021, 2021.

536 Hausfather, Z., Marvel, K., Schmidt, G. A., Nielsen-Gammon, J. W. and Zelinka, M.:
537 Climate simulations: recognize the 'hot model' problem, *Nature*, 605, 26-29. 2022.

538 Hegerl, G.C., F. W. Zwiers, P. Braconnot, N.P. Gillett, Y. Luo, J.A. Marengo Orsini,
539 N. Nicholls, J.E. Penner and P.A. Stott, 2007: Understanding and Attributing
540 Climate Change. In: Climate Change 2007: The Physical Science Basis.
541 Contribution of Working Group I to the Fourth Assessment Report of the
542 Intergovernmental Panel on Climate Change [Solomon, S., D. Qin, M. Manning,
543 Z. Chen, M. Marquis, K.B. Averyt, M. Tignor and H.L. Miller (eds.)]. Cambridge
544 University Press, Cambridge, United Kingdom and New York, NY, USA.

545 Held, I. M., Winton, M., Takahashi, K., Delworth, T., Zeng, F. R. and Vallis, G. K.:
546 Probing the Fast and Slow Components of Global Warming by Returning
547 Abruptly to Preindustrial Forcing, *Journal of Climate*, 23, 2418-2427. 2010.

548 Hienola, A., Partanen, A.-I., Pietikäinen, J.-P., O'Donnell, D., Korhonen, H., Matthews,
549 H. D., and Laaksonen, A.: The impact of aerosol emissions on the 1.5 °C pathways,
550 *Environmental Research Letters*, 13, 044011, 10.1088/1748-9326/aab1b2, 2018.

551 Hoesly, R. M., Smith, S. J., Feng, L., Klimont, Z., Janssens-Maenhout, G., Pitkanen,
552 T., Seibert, J. J., Vu, L., Andres, R. J., Bolt, R. M., Bond, T. C., Dawidowski, L.,
553 Kholod, N., Kurokawa, J. I., Li, M., Liu, L., Lu, Z., Moura, M. C. P., O'Rourke,
554 P. R., and Zhang, Q.: Historical (1750–2014) anthropogenic emissions of reactive
555 gases and aerosols from the Community Emissions Data System (CEDS), *Geosci.
556 Model Dev.*, 11, 369-408, 10.5194/gmd-11-369-2018, 2018.

557 IPCC. Climate Change 2021 – The Physical Science Basis: Working Group I
558 Contribution to the Sixth Assessment Report of the Intergovernmental Panel on
559 Climate Change, 10.1017/9781009157896, 2023.

560 Kristiansen, N. I., Stohl, A. and Wotawa, G.: Atmospheric removal times of the aerosol-
561 bound radionuclides ^{137}Cs and ^{131}I measured after the Fukushima Dai-ichi nuclear
562 accident – a constraint for air quality and climate models, *Atmos. Chem.
563 Phys.*, 12, 10759-10769. 2012.

564 Likens, G. E., Butler, T. J., and Buso, D. C.: Long- and short-term changes in sulfate
565 deposition: Effects of the 1990 Clean Air Act Amendments, *Biogeochemistry*, 52,
566 1-11, 10.1023/a:1026563400336, 2001.

567 Liu, X., Easter, R. C., Ghan, S. J., Zaveri, R., Rasch, P., Shi, X., Lamarque, J. F.,

568 Gettelman, A., Morrison, H., Vitt, F., Conley, A., Park, S., Neale, R., Hannay, C.,
569 Ekman, A. M. L., Hess, P., Mahowald, N., Collins, W., Iacono, M. J., Bretherton,
570 C. S., Flanner, M. G. and Mitchell, D.: Toward a minimal representation of
571 aerosols in climate models: description and evaluation in the Community
572 Atmosphere Model CAM5, *Geoscientific Model Development*, 5, 709-739. 2012.

573 Matsui, H. and Mahowald, N.: Development of a global aerosol model using a two-
574 dimensional sectional method: 2. Evaluation and sensitivity simulations, *Journal*
575 *of Advances in Modeling Earth Systems*, 9, 1887-1920. 2017.

576 Mauritsen, T., Bader, J., Becker, T., Behrens, J., Bittner, M., Brokopf, R., Brovkin, V.,
577 Claussen, M., Crueger, T., Esch, M., Fast, I., Fiedler, S., Flaeschner, D., Gayler,
578 V., Giorgetta, M., Goll, D. S., Haak, H., Hagemann, S., Hedemann, C.,
579 Hohenegger, C., Ilyina, T., Jahns, T., Jimenez-de-la-Cuesta, D., Jungclaus, J.,
580 Kleinen, T., Kloster, S., Kracher, D., Kinne, S., Kleberg, D., Lasslop, G.,
581 Kornblueh, L., Marotzke, J., Matei, D., Meraner, K., Mikolajewicz, U., Modali,
582 K., Moebis, B., Muellner, W. A., Nabel, J. E. M. S., Nam, C. C. W., Notz, D.,
583 Nyawira, S.-S., Paulsen, H., Peters, K., Pincus, R., Pohlmann, H., Pongratz, J.,
584 Popp, M., Raddatz, T. J., Rast, S., Redler, R., Reick, C. H., Rohrschneider, T.,
585 Schemann, V., Schmidt, H., Schnur, R., Schulzweida, U., Six, K. D., Stein, L.,
586 Stemmler, I., Stevens, B., von Storch, J.-S., Tian, F., Voigt, A., Vrese, P., Wieners,
587 K.-H., Wilkenskjeld, S., Winkler, A., and Roeckner, E.: Developments in the MPI-
588 M Earth System Model version 1.2 (MPI-ESM1.2) and Its Response to Increasing
589 CO₂, *J. Adv. Model. Earth Syst.*, 11, 998-1038, 10.1029/2018ms001400, 2019.

590 Morice, C. P., Kennedy, J. J., Rayner, N. A., Winn, J. P., Hogan, E., Killick, R. E.,
591 Dunn, R. J. H., Osborn, T. J., Jones, P. D., and Simpson, I. R.: An Updated
592 Assessment of Near-Surface Temperature Change From 1850: The HadCRUT5
593 Data Set, *Journal of Geophysical Research-Atmospheres*, 126,
594 10.1029/2019jd032361, 2021.

595 Mulcahy, J. P., Jones, C. G., Rumbold, S. T., Kuhlbrodt, T., Dittus, A. J., Blockley, E.
596 W., Yool, A., Walton, J., Hardacre, C., Andrews, T., Bodas-Salcedo, A., Stringer,
597 M., de Mora, L., Harris, P., Hill, R., Kelley, D., Robertson, E., and Tang, Y.:

598 UKESM1.1: development and evaluation of an updated configuration of the UK
599 Earth System Model, *Geosci. Model Dev.*, 16, 1569-1600, 10.5194/gmd-16-1569-
600 2023, 2023.

601 Mulcahy, J. P., Johnson, C., Jones, C. G., Povey, A. C., Scott, C. E., Sellar, A., Turnock,
602 S. T., Woodhouse, M. T., Abraham, N. L., Andrews, M. B., Bellouin, N., Browse,
603 J., Carslaw, K. S., Dalvi, M., Folberth, G. A., Glover, M., Grosvenor, D. P.,
604 Hardacre, C., Hill, R., Johnson, B., Jones, A., Kipling, Z., Mann, G., Molland, J.,
605 O'Connor, F. M., Palmieri, J., Reddington, C., Rumbold, S. T., Richardson, M.,
606 Schutgens, N. A. J., Stier, P., Stringer, M., Tang, Y., Walton, J., Woodward, S.,
607 and Yool, A.: Description and evaluation of aerosol in UKESM1 and HadGEM3-
608 GC3.1 CMIP6 historical simulations, *Geoscientific Model Development*, 13,
609 6383-6423, 10.5194/gmd-13-6383-2020, 2020.

610 O'Neill, B. C., Tebaldi, C., van Vuuren, D. P., Eyring, V., Friedlingstein, P., Hurtt, G.,
611 Knutti, R., Kriegler, E., Lamarque, J. F., Lowe, J., Meehl, G. A., Moss, R., Riahi,
612 K., and Sanderson, B. M.: The Scenario Model Intercomparison Project
613 (ScenarioMIP) for CMIP6, *Geosci. Model Dev.*, 9, 3461-3482, 10.5194/gmd-9-
614 3461-2016, 2016.

615 Ohara, T., Akimoto, H., Kurokawa, J., Horii, N., Yamaji, K., Yan, X., and Hayasaka,
616 T.: An Asian emission inventory of anthropogenic emission sources for the period
617 1980-2020, *Atmospheric Chemistry and Physics*, 7, 4419-4444, 10.5194/acp-7-
618 4419-2007, 2007.

619 Samset, B. H., Sand, M., Smith, C. J., Bauer, S. E., Forster, P. M., Fuglestvedt, J. S.,
620 Osprey, S., and Schleussner, C.-F.: Climate Impacts From a Removal of
621 Anthropogenic Aerosol Emissions, *Geophysical Research Letters*, 45, 1020-1029,
622 <https://doi.org/10.1002/2017GL076079>, 2018.

623 Seland, Ø., Bentsen, M., Olivié, D., Toniazzo, T., Gjermundsen, A., Graff, L. S.,
624 Debernard, J. B., Gupta, A. K., He, Y. C., Kirkevåg, A., Schwinger, J., Tjiputra,
625 J., Aas, K. S., Bethke, I., Fan, Y., Griesfeller, J., Grini, A., Guo, C., Ilicak, M.,
626 Karset, I. H. H., Landgren, O., Liakka, J., Moseid, K. O., Nummelin, A.,
627 Spensberger, C., Tang, H., Zhang, Z., Heinze, C., Iversen, T., and Schulz, M.:

628 Overview of the Norwegian Earth System Model (NorESM2) and key climate
629 response of CMIP6 DECK, historical, and scenario simulations, *Geosci. Model*
630 *Dev.*, 13, 6165-6200, 10.5194/gmd-13-6165-2020, 2020.

631 Sellar, A. A., Jones, C. G., Mulcahy, J. P., Tang, Y., Yool, A., Wiltshire, A., O'Connor,
632 F. M., Stringer, M., Hill, R., Palmieri, J., Woodward, S., de Mora, L., Kuhlbrodt,
633 T., Rumbold, S. T., Kelley, D. I., Ellis, R., Johnson, C. E., Walton, J., Abraham,
634 N. L., Andrews, M. B., Andrews, T., Archibald, A. T., Berthou, S., Burke, E.,
635 Blockley, E., Carslaw, K., Dalvi, M., Edwards, J., Folberth, G. A., Gedney, N.,
636 Griffiths, P. T., Harper, A. B., Hendry, M. A., Hewitt, A. J., Johnson, B., Jones,
637 A., Jones, C. D., Keeble, J., Liddicoat, S., Morgenstern, O., Parker, R. J., Predoi,
638 V., Robertson, E., Siahaan, A., Smith, R. S., Swaminathan, R., Woodhouse, M. T.,
639 Zeng, G., and Zerroukat, M.: UKESM1: Description and Evaluation of the UK
640 Earth System Model, *J. Adv. Model. Earth Syst.*, 11, 4513-4558,
641 10.1029/2019ms001739, 2019.

642 Smith, C. J. and Forster, P. M.: Suppressed Late-20th Century Warming in CMIP6
643 Models Explained by Forcing and Feedbacks, *Geophysical Research Letters*, 48,
644 10.1029/2021gl094948, 2021.

645 Steffen, W., Crutzen, P. J., and McNeill, J. R.: The Anthropocene: Are humans now
646 overwhelming the great forces of nature, *Ambio*, 36, 614-621, 10.1579/0044-
647 7447(2007)36[614:taahno]2.0.co;2, 2007.

648 Tatebe, H., Ogura, T., Nitta, T., Komuro, Y., Ogochi, K., Takemura, T., Sudo, K.,
649 Sekiguchi, M., Abe, M., Saito, F., Chikira, M., Watanabe, S., Mori, M., Hirota, N.,
650 Kawatani, Y., Mochizuki, T., Yoshimura, K., Takata, K., O'Ishi, R., Yamazaki, D.,
651 Suzuki, T., Kurogi, M., Kataoka, T., Watanabe, M., and Kimoto, M.: Description
652 and basic evaluation of simulated mean state, internal variability, and climate
653 sensitivity in MIROC6, *Geoscientific Model Development*, 12, 2727-2765,
654 10.5194/gmd-12-2727-2019, 2019.

655 Tegen, I., Neubauer, D., Ferrachat, S., Siegenthaler-Le Drian, C., Bey, I., Schutgens,
656 N., Stier, P., Watson-Parris, D., Stanelle, T., Schmidt, H., Rast, S., Kokkola, H.,
657 Schultz, M., Schroeder, S., Daskalakis, N., Barthel, S., Heinold, B. and Lohmann,

658 U.: The global aerosol-climate model ECHAM6.3-HAM2.3-Part 1: Aerosol
659 evaluation, *Geoscientific Model Development*, 12, 1643-1677. 2019.

660 Textor, C., Schulz, M., Guibert, S., Kinne, S., Balkanski, Y., Bauer, S., Berntsen, T.,
661 Berglen, T., Boucher, O., Chin, M., Dentener, F., Diehl, T., Easter, R., Feichter,
662 H., Fillmore, D., Ghan, S., Ginoux, P., Gong, S., Kristjansson, J. E., Krol, M.,
663 Lauer, A., Lamarque, J. F., Liu, X., Montanaro, V., Myhre, G., Penner, J., Pitari,
664 G., Reddy, S., Seland, O., Stier, P., Takemura, T. and Tie, X.: Analysis and
665 quantification of the diversities of aerosol life cycles within AeroCom,
666 *Atmospheric Chemistry and Physics*, 6, 1777-1813. 2006.

667 Vestreng, V., Myhre, G., Fagerli, H., Reis, S., and Tarrasón, L.: Twenty-five years of
668 continuous sulphur dioxide emission reduction in Europe, *Atmos. Chem. Phys.*, 7,
669 3663-3681, 10.5194/acp-7-3663-2007, 2007.

670 Wang, Z., Lin, L., Xu, Y., Che, H., Zhang, X., Zhang, H., Dong, W., Wang, C., Gui,
671 K., and Xie, B.: Incorrect Asian aerosols affecting the attribution and projection
672 of regional climate change in CMIP6 models, *Npj Climate and Atmospheric
673 Science*, 4, 10.1038/s41612-020-00159-2, 2021.

674 Watterson, I. G. and Dix, M. R.: Effective sensitivity and heat capacity in the response
675 of climate models to greenhouse gas and aerosol forcings, *Quarterly Journal of the
676 Royal Meteorological Society*, 131, 259-279. 2005.

677 Wilcox, L. J., Highwood, E. J., and Dunstone, N. J.: The influence of anthropogenic
678 aerosol on multi-decadal variations of historical global climate, *Environmental
679 Research Letters*, 8, 10.1088/1748-9326/8/2/024033, 2013.

680 Wu, T., Zhang, F., Zhang, J., Jie, W., Zhang, Y., Wu, F., Li, L., Yan, J., Liu, X., Lu,
681 X., Tan, H., Zhang, L., Wang, J., and Hu, A.: Beijing Climate Center Earth System
682 Model version 1 (BCC-ESM1): model description and evaluation of aerosol
683 simulations, *Geosci. Model Dev.*, 13, 977-1005, 10.5194/gmd-13-977-2020, 2020.

684 Yukimoto, S., Kawai, H., Koshiro, T., Oshima, N., Yoshida, K., Urakawa, S., Tsujino,
685 H., Deushi, M., Tanaka, T., Hosaka, M., Yabu, S., Yoshimura, H., Shindo, E.,
686 Mizuta, R., Obata, A., Adachi, Y., and Ishii, M.: The Meteorological Research
687 Institute Earth System Model Version 2.0, MRI-ESM2.0: Description and Basic

688 Evaluation of the Physical Component, Journal of the Meteorological Society of
689 Japan, 97, 931-965, 10.2151/jmsj.2019-051, 2019.

690 Zhang, J., Furtado, K., Turnock, S. T., Mulcahy, J. P., Wilcox, L. J., Booth, B. B.,
691 Sexton, D., Wu, T., Zhang, F., and Liu, Q.: The role of anthropogenic aerosols in
692 the anomalous cooling from 1960 to 1990 in the CMIP6 Earth System Models,
693 Atmos. Chem. Phys. Discuss., 1-39, 10.5194/acp-2021-570, 2021a.

694 Zhang, J., Wu, T., Zhang, F., Furtado, K., Xin, X., Shi, X., Li, J., Chu, M., Zhang, L.,
695 Liu, Q., Yan, J., Wei, M., and Ma, Q.: BCC-ESM1 Model Datasets for the CMIP6
696 Aerosol Chemistry Model Intercomparison Project (AerChemMIP), Advances in
697 Atmospheric Sciences, 38, 317-328, 10.1007/s00376-020-0151-2, 2021b.